Optimal shape design of shoulder fillets for flat and round bars under various loadings

F O Sonmez
Department of Mechanical Engineering, Bogazici University, Bebek 34342, Istanbul, Turkey.
email: sonmezfa@boun.edu.tr

The manuscript was received on 25 November 2008 and was accepted after revision for publication on 24 February 2009.

DOI: 10.1243/09544062JMES1457

Abstract: Fillets are usually the most critical regions in mechanical parts especially under fatigue loading, considering that an increase in the maximum stress level considerably shortens the fatigue life of a part. The aim of this study is to find the best shape for a fillet in a shouldered shaft or plate so that the maximum equivalent stress has the lowest possible value.

Optimization is achieved using a stochastic global search algorithm called the direct search simulated annealing. The boundary is defined using spline curves passing through a number of key points. The method is also applicable to shape optimization problems in which geometric constraints are imposed and, for this reason, tangential stress is not uniform along the optimal fillet boundary. Optimal shapes are obtained for flat and round bars subject to axial, bending, torsional, or combined loads. The results show that stress concentration factors close to one can be achieved even for bars with significant variations in cross-section. Besides, the region occupied by the optimum fillets is much smaller in comparison to circular or elliptical ones.

Keywords: shape optimization, global optimum, stress concentration, direct search simulated annealing, finite element model

1 INTRODUCTION

Fillets are commonly used in mechanical parts to provide smooth transition in regions where there is a sudden change in cross-section as in the case of shoulders. Shoulders are introduced in bars for various purposes, to provide bearing support, cam profile, etc. However, this leads to an increase in local stress levels. Stress concentration factor K_t, which is the ratio of the maximum stress developed in this region, σ_{max}, to nominal stress σ_o, is a measure of this increase

$$K_t = \frac{\sigma_{max}}{\sigma_o} \tag{1}$$

The usual practice in machine design is to use a circular profile for fillets. As Fig. 1 indicates, a larger reduction ratio, D/d, or a smaller radius of curvature of the fillet, r, results in a higher stress concentration. In many cases, choosing a large radius of curvature may not be possible because of space limitations or existence of a nearby mechanical part. For that reason, critical stresses are expected to develop at the fillets. In the case of fluctuating loads, high stresses developed in the fillets may lead to premature fatigue failure, considering that fatigue crack initiation is quite sensitive to stress level.

Circular or elliptical profiles are not optimal as shown before [**1**]. They have much higher stress concentration factors, K_t, in comparison to optimal shapes. These profiles lead to high stress concentration and therefore considerably weaken the part. It is possible to significantly reduce the peak stress level, thus increasing the fatigue strength of mechanical parts through shape optimization. Accordingly, the problem considered in this study is to find the globally optimum shapes for the fillets that will result in the lowest possible stress concentration.

Many researchers attempted to obtain optimum shape designs of shoulder fillets [**1**–**35**]. Some of them [**10**, **13**, **15**, **16**, **21**–**25**, **34**] minimized fillet area, while keeping stress concentration below a limit. Others [**2**, **3**, **5**, **8**, **14**, **18**, **26**, **31**–**33**] minimized the maximum stress at the shoulder. Hedia [**20**] reduced fatigue notch factor, Das *et al.* [**27**] and Jones *et al.* [**24**, **28**] reduced stress intensity factor at the fillet. Another approach in the previous studies [**1**, **7**, **19**, **29**, **35**] is to make the tangential stress uniform along the fillet boundary,

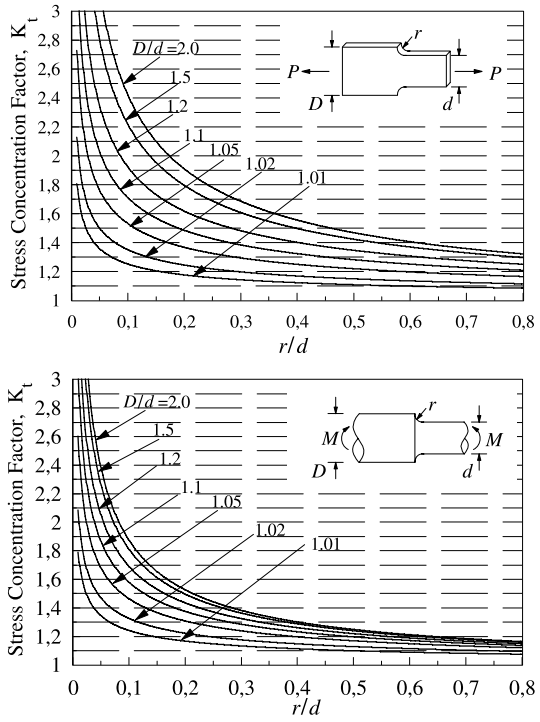

Fig. 1 Stress concentration factors for shoulder fillets in flat and round bars. Analytical formulae given in reference [**36**] were used to generate the curves

assuming this is consistent with the aim of minimizing the peak stress. This approach seems to be much more successful in reducing stress concentration as the comparisons of the results provided by Waldman *et al.* [**1**] and Pedersen [**35**] suggest. Besides, this method is computationally efficient. One should note that this method is applicable to shape optimization problems in which no geometric constraint exists. In many machine design applications, however, the geometry of a part is constrained by neighbouring parts. Its boundary may not infringe on the boundaries of other parts. In these cases, one may not assume constant tangential stress along the boundary of the optimal shape.

In this study, a new procedure is proposed to generate improved results in some respects. First of all, because directly the peak stress is minimized, the method is applicable to problems in which geometrical constraints are imposed and, for this reason, tangential stress is not uniform along the optimal fillet boundary as shown in one example problem. Second, in shape optimization problems, there exist many locally optimum designs [**37**, **38**], which may be far worse than the globally optimum design according to the chosen criterion of effectiveness. For that reason, a downhill proceeding algorithm, in which a monotonically decreasing value of objective function is iteratively created, may get stuck into a locally minimum point other than the globally minimum one. To find the absolute minimum of an objective function without being sensitive to starting position, a global optimization method has to be employed in structural optimization problems. If a local-search algorithm is used, as in many of the previous studies, an optimization procedure can only be successful if it is used to improve a current design. In that case, the resulting shape depends on the initial shape, thus on designer's intuition; therefore, it may not reflect the best possible design. In this study, a reliable global search algorithm called 'the direct search simulated annealing (DSA)' [**39**] was used. Hence, the optimization algorithm may start from almost any initial model, search a large design domain, and find the globally optimum design. Although stochastic search algorithms are computationally inefficient, they are applicable to optimization problems that involve analysis of small linearly elastic structures like shouldered shafts, which can be carried out in a few seconds even by an ordinary computer.

Third, searching for the best possible shape is viable only with a precise definition of boundary. The shape of a structure (i.e. its outer boundary) is defined by a number of variables in a shape optimization process. If different values are chosen for these variables, a different shape is obtained. If the definition of boundary is based on a limited number of design variables, and thus it allows generation of only a limited number of distinct shapes, the algorithm may not find the best possible shape, because it may not be possible to define it by the chosen design variables. Although Shim and Manoochehri [**13**] used simulated annealing (SA) to generate globally optimum shapes, and obtained quite promising results starting from arbitrary designs, their definition of shape was not precise enough. In their approach, a structure was first divided into a number of small finite-element blocks and then these blocks were randomly removed or restored to obtain randomly generated shapes. Precise definition of boundary required a very fine finite-element mesh, but this was not possible because of the computational burden. Fourth, another concern in shape optimization is the accuracy, i.e. how well the optimum shape found by the search algorithm represents the best possible shape. In many of the previous studies, the accuracy remained questionable. In this study, a method was proposed to ensure precise definition of the boundary. A more precise definition requires larger numbers of design variables, which makes it more difficult and time consuming for the optimization algorithm to locate the globally optimum design. Consequently, the accuracy of the results obtained using a large number of design parameters would be questionable. However, the proposed method ensures precision without compromising from the accuracy.

Fatigue failure is the most critical failure mode in shouldered power transmission shafts. Minimizing stress concentration at fillets is especially crucial in this type of applications. Yet, optimum shape design of shoulder fillets in round bars has rarely been studied

[**4**, **6**, **7**]. Most of the previous studies [**1**–**3**, **5**, **8**–**35**] considered only shouldered flat bars even though the engineering applications involving flat bars susceptible to fatigue failure are comparatively quite rare. Besides, in most of the previous studies, only axial loading was considered. In this study, in addition to flat bars, optimal design of shouldered round bars was investigated. All the relevant load cases (axial force, pure bending, torsion, transverse force, and combined loading) were considered.

2 PROBLEM STATEMENT

Figure 2 depicts fillet shape optimization problem for a shouldered plate under axial loading. σ_0 is the far field stress. The geometric features having determining effect on stress concentration factor are the ratios of D/d and $\ell/(D-d)$ [**1**] and most importantly the shape of the fillet. ℓ is the length of the transition region.

If a bar is subject to axial loading or bending moment, the stress concentration factor is usually defined as the ratio of the largest first principal stress σ_1 at the fillet to the nominal stress S_{nom} [**40**, **41**]

$$K_{\text{t}} = \frac{\sigma_1}{S_{\text{nom}}} \tag{2}$$

Nominal stress S_{nom} is calculated using the formula $4P/\pi d^2$ for an axial load P and $32M/\pi d^3$ for a bending moment M. If the bar is subject to torsion, K_{t} is defined as the ratio of the maximum shear stress in the fillet, $\tau_{\max}$, to the nominal shear stress τ_{nom} [**41**]

$$K_{\text{t}} = \frac{\tau_{\max}}{\tau_{\text{nom}}} \tag{3}$$

The nominal shear stress τ_{nom} is calculated using the formula $16T/\pi d^3$.

One should note that even though the far field stress is uniaxial, multiaxial stress state may develop at the fillet; besides, in many applications a combined loading is applied. If the part is subject to fluctuating loads, its fatigue life depends on the magnitude of the equivalent (Von Mises) stress rather than on a single component of stress. For this reason, a definition of

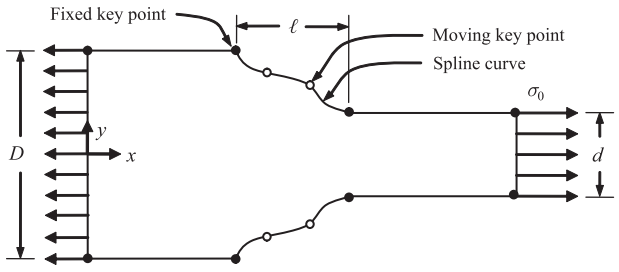

Fig. 2 Representation of a fillet shape optimization problem for a shouldered plate

stress concentration factor based on equivalent stress is used in this study

$$K_{\text{q}} = \frac{(\sigma_{\text{q}})_{\max}}{\sigma_{\text{nom}}} \tag{4}$$

where $(\sigma_{\text{q}})_{\max}$ is the maximum equivalent stress in the fillet. The nominal stress σ_{nom} is also calculated based on the equivalent stress. Because σ_{nom} is constant, minimization of the peak equivalent stress induced in the structure consequently minimizes K_{q}. The objective function may then be expressed in the following form

$$f = \frac{(\sigma_{\text{q}})_{\max}}{\sigma_{\text{allow}}} \tag{5}$$

where σ_{allow} is the allowable stress. $(\sigma_{\text{q}})_{\max}$ is divided by σ_{allow} to normalize the objective function.

One should note that if the part were subject to static loads and made of a brittle material, tensile stresses would be more damaging. In that case, minimizing the maximum tensile stress rather than the equivalent stress would be more effective in increasing the performance of the part.

Shape optimization requires definition of shape in terms of optimization variables. The search algorithm tries to find the optimum values of these variables. Shape of a two-dimensional (2D) structure is defined by its thickness and the boundary of its lateral area; shape of an axisymmetric structure is defined by its symmetry axis and the boundary of its axisymmetric section. Accordingly, their boundaries, thus their shapes, can easily be described by spline curves passing through a number of key points. Some of these points may be fixed, while the others are allowed to move during optimization. The initial positions of the key points, including fixed and moving, are given at the start and the boundary of the initial model is formed by joining these key points by lines or spline curves. Whenever the positions of the moving key points are changed, a new boundary, a new shape is obtained. Accordingly, the x- and y-coordinates of the moving key points become optimization variables. There are some restrictions on the movements of the key points, i.e. constraints on the optimization variables. First of all, the key points are allowed to move only within a search region S defined by the designer. Although search of the globally optimum design without restricting the movements of the key points is possible, computational time becomes unnecessarily much longer. Search domain should not be too restrictive, but should exclude the regions that are definitely expected to be away from the optimum boundary. As another constraint, no part of the structure is to lose its connection to the restraints, i.e. the structure should remain in one piece. After the movement of key points if one segment of the boundary crosses another one, or they touch each other, connectivity is lost. These are

the two constraints imposed on the optimization variables. Any movement of the key points violating these constraints is not to be accepted during optimization. The optimization problem may then be expressed as

Given: Initial positions of key points and how they are connected, boundary conditions (applied forces and restraints), and material properties.
Find: The globally optimum shape of the structure.
Minimize: Maximum equivalent stress $(\sigma_q)_{max}$.
Subject to: The geometric constraints (model connectivity and search domain).
Design variables: The coordinates of the moving key points.

3 OPTIMIZATION PROCEDURE

3.1 Application of a direct search-simulated annealing algorithm to shape optimization

In this study, the DSA, proposed by Ali *et al.* [**39**], was adopted as the search algorithm. This is an improved variant of the SA algorithm. The application of DSA to shape optimization was explained in detail in a previous study [**37**]. In this study, a number of improvements were introduced to increase the reliability of the algorithm and reduce computational cost.

In DSA, unlike ordinary SA, a set of current configurations rather than a single current configuration is maintained during the optimization process. This feature is similar to the use of population in genetic algorithms. Hence, unlike the standard SA algorithm where only the neighbourhood of a single point is searched, DSA searches the neighbourhood of all the current points in the set. Accordingly, at the start of the optimization process, N is the number of initial configurations created by randomly selecting the positions of the key points within the search region. N is equal to $7(n+1)$, where n is the number of optimization variables. Since x- and y-coordinates of the moving key points are the variables defining the fillet shape, in our case n is equal to two times the number of moving key points.

DSA like SA seeks the global optimum through randomly generated configurations. Shape optimization through DSA thus requires generation of random shapes. This is achieved by changing the positions of the key points in random directions through random distances. In each iteration, a new configuration is randomly generated in the neighbourhood of a randomly chosen current configuration by giving random movements to its key points. The coordinates of the ith key point (x_i', y_i') of the new configuration are calculated as

$$x_i' = x_i + c_r R_{max} \cos(\theta_r)$$
$$y_i' = y_i + c_r R_{max} \sin(\theta_r) \tag{6}$$

where (x_i, y_i) are the coordinates of the ith key point of the randomly chosen current configuration, c_r is a random number between 0.0 and 1.0, θ_r is a random number between 0.0 and 2π, and R_{max} is the maximum moving distance. To search the global optimum within a large region, instead of giving small perturbations to the current configuration to obtain a new configuration in its near neighbourhood, one should allow a large variance in the current configurations. This is achieved by assigning a large value to R_{max}.

Acceptability of a newly generated trial configuration, A_t, is calculated by

$$A_t = \begin{cases} 1 & \text{if } f_t \leqslant f_h \\ \exp((f_h - f_t)/T_j) & \text{if } f_t > f_h \end{cases} \tag{7}$$

Here f_t is the cost of the newly generated configuration as calculated by equation (5) and f_h is the highest cost in the current set. This means that every new design having a cost lower than the cost of the worst design is accepted. But, if the cost is higher, the trial configuration may be accepted depending on the value of A_t. If it is greater than a randomly generated number, P_r, the trial configuration is accepted, otherwise it is rejected. If the trial design is accepted, it replaces the worst configuration. Because SA allows acceptance of configurations with a higher cost, local minimum designs can be avoided through such uphill moves. As equation (7) implies, if the value of T is high, the probability that a worse configuration is accepted will also be high. The initial value of T should be so high that nearly all trials can be accepted. Generating arbitrary configurations in the neighbourhood of the current ones, accepting any arbitrary configuration and repeating these iterations many times allow the whole feasible domain to be thoroughly searched at the initial stages of optimization. In the physical analogy, choosing high T_o corresponds to heating up the solid until all particles are randomly arranged in the liquid phase such that atoms may freely arrange themselves.

Iterations during which the value of the temperature parameter T is kept constant are called Markov chains (or inner loops). Ali *et al.* [**39**] adopted the following formula to decide on the length of a Markow chain (the number of trials (or iterations)) for the kth level of T

$$L_k = L + L(1 - e^{f_l - f_h}) \tag{8}$$

where

$$L = 10n \tag{9}$$

Here n is the number of optimization variables. At high temperatures, the current configurations form a sparse cluster; they are scattered all over the design domain; consequently, f_h–f_ℓ is large and Markow chain length is close to $2L$. On the other hand, when

they form a dense cluster at low temperatures, it approaches L. The temperature parameter T is continually reduced during the optimization process. Iterations are continued until the difference between the costs of the best and worst current configurations becomes small.

As in the physical annealing process, where the mobility of the atoms diminishes during cool down, mobility of the key points is decreased as acceptability decreases. The configuration that is worse than all current configurations except the worst one is defined as the worse configuration, and if no improvement is made on the worse shape during a Markow chain, $R_{\max}$ is reduced by

$$R_{\max} = \beta R_{\max} \tag{10}$$

where the coefficient β was chosen to be 0.995. In this way, the neighbourhood of the current configurations within which a new configuration is generated narrows down as acceptability becomes lower and lower.

3.2 Ensuring precision and accuracy

If optimal shapes are obtained using a low number of moving key points, definition of the boundary will be imprecise, but the globally optimal shape can reliably be obtained to a high degree of accuracy. However, an imprecisely defined optimal shape even if it is globally optimum for the chosen design variables may not represent the best possible shape. If the number of key points is increased, the boundary can be defined more precisely, but the reliability of the algorithm in finding the globally optimal design becomes questionable. This is because the likelihood of getting stuck into a local optimum will be high with a large number of optimization variables even if a global search algorithm is used. However, if some regions of the search domain that are expected to be away from the globally optimal boundary are excluded, reliability of the search algorithm can be increased. Restricting the search domain for a more precisely defined shape design problem by considering the optimal shape obtained using a lower number of key points, one may obtain a higher reliability. By successively generating more and more precise optimal shapes and each time restricting the search domain, one may locate the best possible shape as shown in the following shape design problems.

4 RESULTS AND DISCUSSION

4.1 Shouldered flat bars under axial loading

The optimization procedure was applied through a computer code developed using ANSYS Parametric Design Language. The shape optimization algorithm was first applied to a plate with a shoulder subject to axial loading as shown in Fig. 3. In this structure, there is a significant variation in cross-section, the width of the larger portion is 40 mm and that of the smaller portion is 20 mm. K_q is independent of the material in the linearly elastic range and the level of stress. The flat bar is in plane-stress condition. As long as the thickness is not large enough to invalidate the plane stress assumption, it does not affect K_q. The geometric proportions affecting stress concentration take the values $D/d = 2$ and $\ell/(D-d) = 0.75$. Although, this geometry seems to be not practical and rarely used by the designers, this is one of the common geometries adopted in the previous studies of shape optimization. To be able to compare the results, and appreciate the relative advantage gained by the method proposed in this study, this geometry was adopted.

Initially, the boundary in the transition region is defined using two moving key points. These key points are allowed to move only within the search domain shown in the figure. The right edge is fixed in length and subjected to 300 MPa pressure, while the left edge is restrained from movement in the x-direction. The material of the structure is steel with an elastic modulus of 207 MPa and Poisson's ratio of 0.28.

Taking advantage of symmetry, only the upper portion was analysed to save computational time and its bottom was restrained from moving in the y-direction due to the symmetry condition. Figure 4 shows the finite-element mesh of one of the initial models randomly generated at the start of the optimization process. Six-node triangular elements having two degrees of freedom (Plane2 element of ANSYS with the plane stress option) were used in the finite-element models (FEMs). The meshes near the moving segment of the boundary were refined to correctly determine the stress state in this region where high stresses were expected to develop. As shown in the previous study [**37**], accuracy of the finite-element (FE) solution considerably affects the resulting optimum shape. To ensure the accuracy at which the objective function f was calculated, convergence of the FE solution was frequently checked during the optimization process. If the change in the magnitude of the maximum stress was greater than 0.3 per cent when FE analysis of currently best configuration was carried out using one-fourth of the current size of finite elements, then the FE mesh was refined. Towards the end of the optimization process, the element size became about one-fourth of the size of the elements shown in Fig. 4 due to occasional refinements. The horizontal length of the model was chosen to be large enough to limit the edge effects on the stress state at the fillet. Thus, even if a longer portion of the plate was analysed, the change in the stress state would be negligible (<0.3 per cent).

First, the shape of the fillet defined by two moving key points was optimized following the optimization procedure described above. Figure 5 shows the

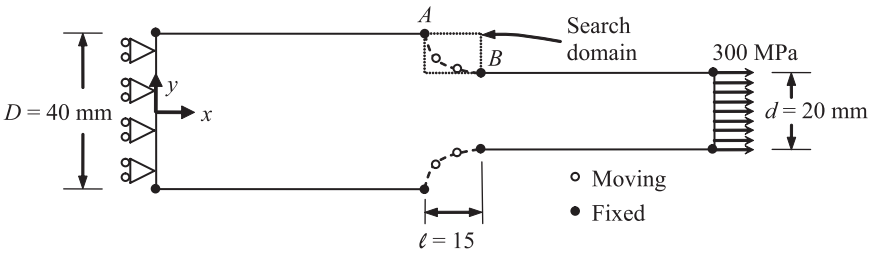

Fig. 3 Shouldered plate subject to axial loading

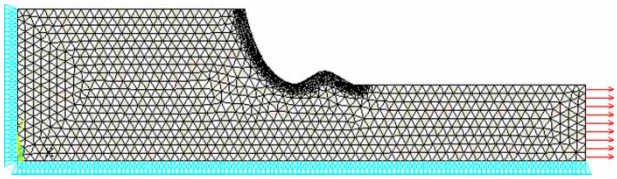

Fig. 4 One of the initial configurations of the shouldered plate with its mesh

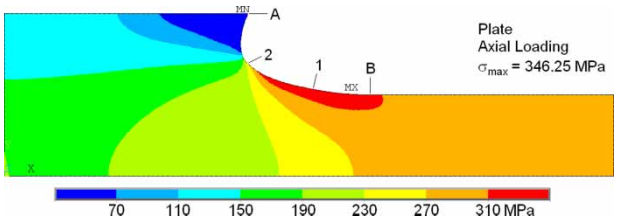

Fig. 5 Stress distribution within the optimal-shaped plate with a shoulder fillet defined by two key points

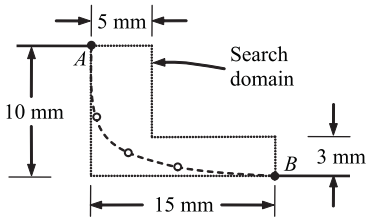

Fig. 6 Search domain used for three moving key points

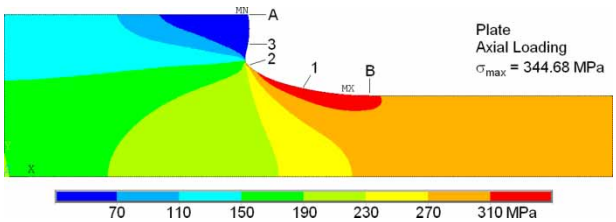

Fig. 7 Stress distribution within the optimal-shaped plate with a shoulder fillet defined by three key points

optimal shape of the fillet and the stress distribution within the plate. The maximum equivalent stress, $(\sigma_q)_{max}$, is 346.25 MPa. '*B*' indicates the position of the fixed key point at the right end of the transition region shown in Fig. 3, while '1' and '2' point to the optimal positions of the moving key points.

The optimal shape obtained by two moving key points implies that the search region shown in Fig. 3 is unnecessarily large. Movements of the key points toward the region around the upper right corner certainly result in worse designs. Inclusion of this region within the search domain leads to generation of many unnecessary configurations, and thus high computational cost. For this reason, the search domain shown in Fig. 6 was adopted in the optimization of the fillet defined by three key points. However, the optimum fillet shape obtained with two key points was not used as an initial configuration in the new optimization process. Again, the initial coordinates of the moving key points were randomly generated within the search domain. The resulting optimal-shaped plate and the stress state are shown in Fig. 7. The maximum equivalent stress $(\sigma_q)_{max}$ turned out to be 344.68 MPa. Because three key points provided a more precise definition of shape, allowing generation of shapes not possible with two key points, a better shape with a lower stress concentration was obtained.

Next, the fillet shape defined by four key points was optimized. This time, a separate search domain was used for each key point (Fig. 8). This eliminates generation of very irregular shapes, but allows generation of every possible near optimum shape. If a key point gets close to its border during the optimization process in all of the current configurations, its search domain was expanded. If a key point gets away from one of the border lines of its search domain, then this line is moved closer. Figure 9 shows the optimal shape and the stress state in the plate. The maximum stress is 340.84 MPa. Unlike the previous shapes, a protrusion

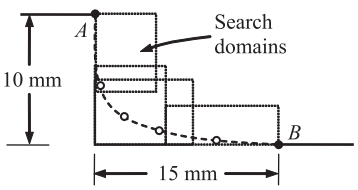

Fig. 8 Separate search domains for four moving key points

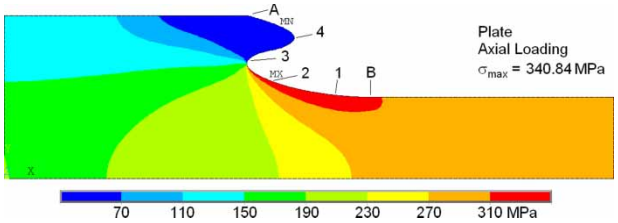

Fig. 9 Stress distribution within the optimal-shaped plate with a shoulder fillet defined by four key points

develops at the upper portion of the fillet. Because the algorithm tries to minimize the maximum stress and this is a lower stressed region, one may assume that the algorithm places the third and fourth key points to provide a better curvature in the highly stressed lower portion of the fillet rather than to minimize stresses in the upper portion. Accordingly, in these three trials, although the shapes of the upper portion are quite different, the lower portions are quite similar as seen in Figs 5, 7, and 9.

The fillet shape was then defined more precisely by six key points. Because such a high number of key points may lead to generation of very irregular shapes that are difficult to analyse by FEM, a small and separate search domain was defined for each key point (Fig. 10). To decide on the location and size of the search domains, the optimal fillet shape defined by four key points was used. However, initial positions of the key points were again arbitrarily chosen by the algorithm within the search domains. Figure 11 shows the optimal shape and the stress distribution in the plate. The maximum equivalent stress is 340.00 MPa.

Finally, the number of key points was increased to eight, and the fillet shape was optimized. This time,

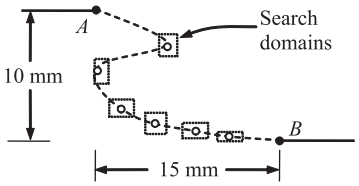

Fig. 10 Separate search domains for six moving key points

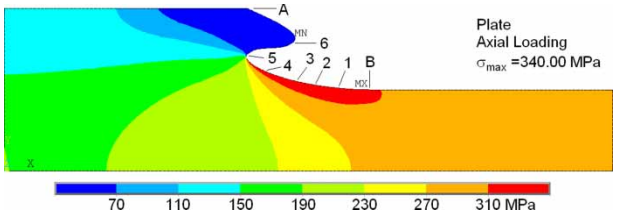

Fig. 11 Stress distribution within the optimal-shaped plate with a shoulder fillet defined by six key points

the maximum equivalent stress developed in the plate was 339.62 MPa. One may still find a better shape by further increasing the number of moving key points; however, the small gain thus achieved does not justify the increased computational effort.

To validate the assumption that a protrusion was formed in the lower stressed region to provide the optimal curvature in the highly stressed region, this protrusion was removed and an FE analysis of the remaining plate was carried out. As seen in Fig. 12, the same stress state was obtained. Assuming that increasing the number of key points further does not lead to appreciable improvement in the objective function f, one may consider the plate with the protrusion removed as the optimal shape. In that case, the stress concentration factor K_q, calculated for the optimum shape, is equal to 1.132. Considering that D/d ratio of the plate, which is 2.0, is quite large, one may not obtain such low values with circular fillet profiles except for very large fillet radii. This is also lower than the ones that were found in the previous studies. Waldman *et al.* [**36**] obtained lower values of stress concentration factors in comparison to the ones obtained in the previous studies of shape optimization. For the same geometry, they obtained an optimal shape with a concentration factor of 1.146.

To compare the stress concentration factors of the circular and optimum shapes, a shouldered plate with a circular fillet was analysed. About the same length (15 mm) was chosen for the transition region. This meant a fillet radius of 16 mm ($r/d = 0.80$). The other geometric parameters ($D/d = 2.0$) and boundary conditions were chosen to be the same. Figure 13 shows the stress state in the plate. The maximum equivalent

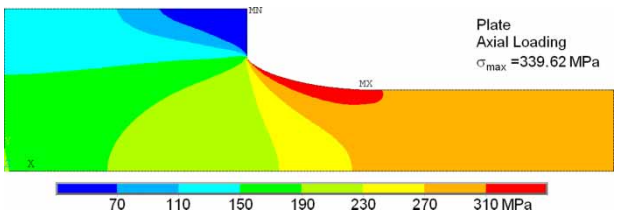

Fig. 12 Stress distribution within the optimal-shaped plate with a shoulder fillet defined by eight key points. The protruding portion was removed

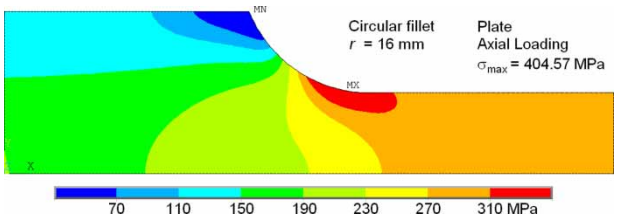

Fig. 13 Stress distribution developed in a shouldered plate with a circular fillet having a radius of curvature of 16 mm

stress is 404.57 MPa. This means that the stress concentration factor, K_q, is equal to 1.349. This is much higher (∼19 per cent) than the one for the optimum shape. Another advantage of using the optimum fillet design is that the region occupied by the fillet is much smaller.

4.2 Comparison of the results

Table 1 shows a comparison of the published values of stress concentration factors and the ones obtained in the present study. Actually, the results are not exactly comparable. First of all, the objective functions are differently formulated in those studies. The researchers used tangential stress, axial stress, or equivalent stress in their definition of stress concentration factor. However, the resulting differences in the values of stress concentration factors can be assumed to be small. Second, different FE meshes were used in those studies.

As seen in the table, usually the results of this study are much better than that of the previous studies. Only the present algorithm generated very similar results to that of Pedersen [**35**] and Waldman *et al.* [**36**], who used optimization methods that tried to make the tangential stress at the fillet boundary uniform. Small differences may be attributed to the differences in the finite-elements meshes. Because the accuracy of the finite-element solution is checked during the optimization in the present study, the values of K_q reflect the actual stress concentration. On the other hand, the actual values of K_t or K_q are expected to be higher than the values reported in other studies.

4.3 The effect of accuracy in finite-element calculations

To see the effect of mesh density on the accuracy of the optimal shape, the fillet shape defined by eight key points was optimized using the mesh structure shown in Fig. 14(a). This is actually the same mesh used initially in the other cases except that the same mesh was used throughout the optimization for this case. In other cases, the mesh was refined whenever the error in the finite-element calculations exceeded an acceptable limit as mentioned before. Figure 14(b) shows the stress state in the fillet optimized using the coarse mesh. A lower value, 339.16 MPa, was obtained for the maximum equivalent stress in comparison to the one obtained with a finer mesh (Fig. 12). When the same shape was analysed using the fine mesh shown in Fig. 14(c), a much higher value for the maximum equivalents stress, 355.97 MPa, was calculated (Fig. 14(d)). This shows that the error due to an insufficient mesh density may become unacceptably large and may lead to spurious optimal designs. One should also note that the coarse mesh shown in Fig. 14(a) is even finer than the ones used in many of the previous studies.

Table 1 Comparison of the published optimal stress concentration factors with the ones obtained using the present optimization method

Reference	D/d	ℓ/h	K_q or K_t	Present method, K_q
Waldman *et al.* [**36**]	2.0	1.5	1.146	1.132
Tvergaard[a]	2.0	1.5	1.21	1.132
Miegroet and Duysinx [**33**]	2.0	1.0	1.429	1.249
Pedersen [**35**]	2.0	1.0	1.25	1.249
Waldman *et al.* [**36**]	2.0	1.0	1.242	1.249
Francavilla *et al.* [**2**]	1.667	1.5	1.58	1.216
Bhavikatti and Ramakrishnan[a]	1.667	1.5	1.25	1.216
Waldman *et al.* [**36**]	1.667	1.5	1.210	1.216
Tvergaard[a]	1.5	1.5	1.38	1.278
Waldman *et al.* [**36**]	1.5	1.5	1.272	1.278

[a] Cited in Waldman *et al.* [**36**].

4.4 Optimization with a geometric constraint

In many practical problems of machine design, the part to be designed should fit in a prescribed space and any interference between parts should be avoided. In these cases, a structural optimization procedure for optimal shape design should be able to account for these geometrical constraints. To show that the method proposed in this study is applicable to problems in which geometrical constraints are imposed, a rectangular region around the fillet was defined as infeasible (Fig. 15). During the optimization, if a node on the boundary of a newly generated configuration is within the infeasible domain, this configuration is not accepted and another configuration is regenerated. Figure 15 shows the resulting stress state. Stress concentration is higher in comparison to the unconstrained case (Fig. 12) as expected. Most importantly, the stress is not constant along the transition region. For this reason, the methods that minimize stress concentration by trying to make the tangential stress uniform along the fillet boundary may not work in this case.

4.5 The effect of undercut on optimal shape

The length of the transition region significantly affects the level of the maximum stress. The fillet length in the above problems was taken as 15 mm. If a longer transition region is chosen, one may obtain a lower stress, but at the expense of a larger volume for this region. Increased weight and interference of a nearby mechanical part may then become a problem. As an alternative fillet design, 5 mm of a 30-mm-length transition region was positioned towards the left of the point A as shown in Fig. 16. A 3-mm-length portion of the fillet boundary below this point was fixed to

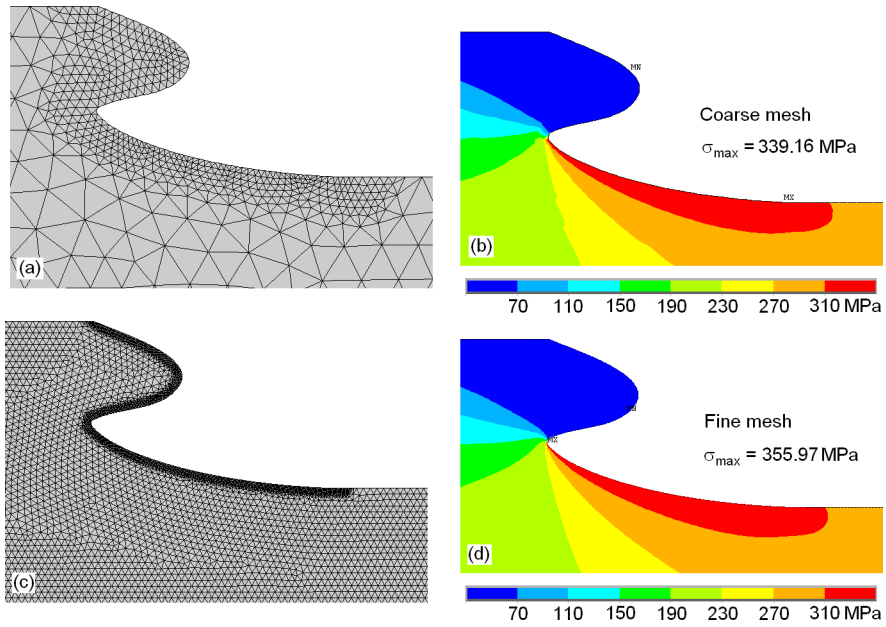

Fig. 14 (b) The stress state at the fillet optimized using the coarse mesh shown in (a). (d) The stress state at the same fillet obtained using the fine mesh shown in (c)

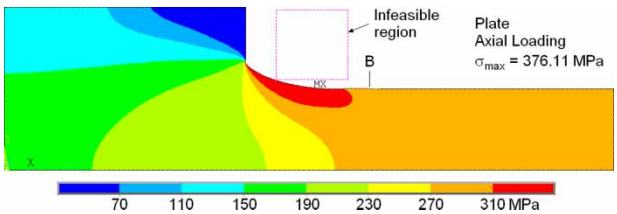

Fig. 15 Fillet shape optimized with a geometric constraint

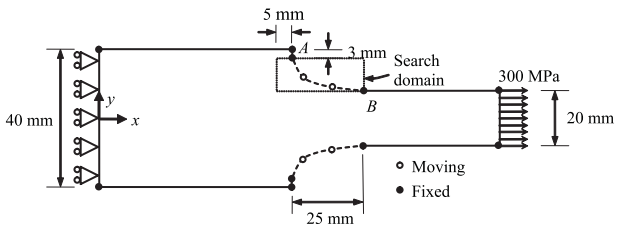

Fig. 16 Shouldered plate subject to axial loading

provide sufficient support. The search domain shown in the figure was initially used in the optimization. Although it is known that undercutting reduces stress concentration for circular fillets, one needs to find out the extent of reduction for optimal fillet shapes. The maximum equivalent stress in the optimal shape design defined by six moving key points was obtained to be 306.68 MPa (Fig. 17). The recess does not weaken the plate, considering that there is no significant loading on this region. Since this is a plate, a recess does not pose any difficulty in manufacturing. On the contrary, this is to the advantage that the fillet occupies a very small space at the shoulder.

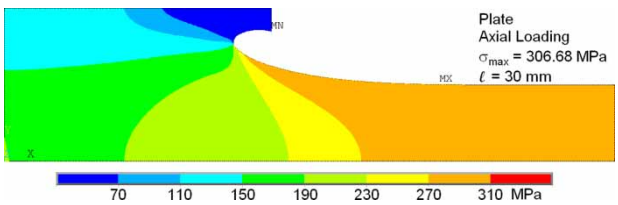

Fig. 17 Stress distribution developed in the optimal-shaped plate with a shoulder fillet defined by six key points

4.6 Shouldered round bars

The next problem considered in this study is the optimum fillet design for a shouldered round bar subject to axial loading. Because this is an axisymmetrical part, the same 2D finite element (Plane2), but with the axisymmetric option, is used. Otherwise, the boundary conditions, the sizes of the fixed portions of the model are the same. Using axisymmetric model greatly reduces the computational time in comparison to an equivalent 3D model. Following the same optimization procedure, the optimum shapes defined by two, three, four, and five moving key points were obtained. The maximum equivalent stresses developed in the optimal shaped bars are 307.02, 306.18, 305.70, and 304.91 MPa (σ_{yy}(max) = 312.95 MPa), respectively. Accordingly, the stress concentration factor for the most precisely defined optimum shaft is 1.016. Again, a protrusion develops in the upper portion of the fillet. Figure 18 shows the stress distribution in the most precisely defined optimal shaft with the protrusion removed. To compare the optimal fillet with the standard circular fillet

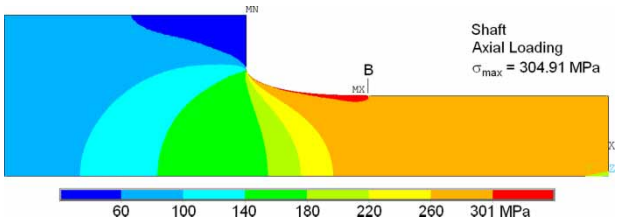

Fig. 18 Stress distribution developed in the optimal-shaped round bar with a 15-mm-shoulder fillet defined by five key points. The protrusion was removed

having the same transition length, analysis of a shouldered shaft having a circular fillet with 16 mm radius of curvature was carried out. The stress state shown in Fig. 19 was obtained. The maximum equivalent stress was 348.74 MPa with $K_q = 1.162$. This means an improvement of about 12 per cent for the optimal shape. Because of the sensitivity of fatigue failure behaviour to stress level, a 12 per cent decrease in maximum stress may result in two times the increase in fatigue life. Besides, the optimal-shaped fillet occupies a much smaller space at the shoulder. In many cases like the use of the shoulder as a bearing seat, this is an important benefit. One should note that the stress concentration factor according to the analytical formula proposed by Noda *et al.* [**1**] is equal to 1.242, which corresponds to a maximum stress of 372.54 MPa. The magnitude of the first principal stress calculated using FEA is 376.13 MPa for the circular fillet of 16 mm radius after setting the Poisson's ratio ν equal to zero. The small difference may be attributed to the error in the analytical formula, which was obtained by making some approximations. FEA results can be assumed to be more accurate.

Next, the shape optimization problem for a shouldered round bar under torsion was considered. Axisymmetric FE models may take non-symmetric loads. Transverse concentrated forces in the z-direction generating 471.24 Nm torque were applied to the right end. Since these forces cannot be continuously distributed in an FE model, pure shear stresses could not be generated at the end. However, conforming to Saint Venant's principle, the stress state

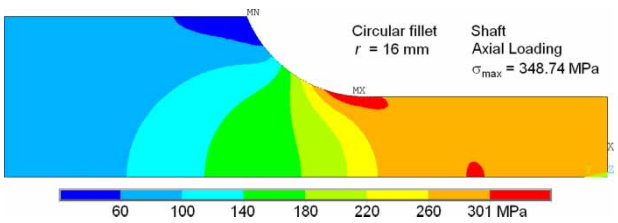

Fig. 19 Stress distribution developed in an axially loaded shouldered round bar with a circular fillet having 16 mm radius of curvature

corresponding to a pure torsional load developed away from the loaded region as shown in Fig. 20. Although the equivalent stress is minimized, τ_{yz} component of stress is displayed. The nominal stress is obtained as 300.00 MPa, which is the same as the value calculated by the well-known formula $\tau_{max} = Tc/J$. K_t is then equal to 1.004. Because the stress concentration factor obtained using three moving key points is very close to 1.0, increasing the number of key points to obtain a more precise definition of the boundary is not needed; in that case only a slight improvement could be achieved. The stress concentration factor K_t for a shouldered shaft with a circular shaft having 16 mm radius of curvature is 1.067. The K_t calculated using the analytical formula [**1**] is 1.09 for this geometry.

The optimization procedure was then applied to a shouldered round bar subject to pure bending. Figure 21 shows the resulting shape and stress distribution. A pure bending moment equal to 235.85 Nm is generated by applying a transverse force couple in the x-direction at the right end of the beam. Away from the

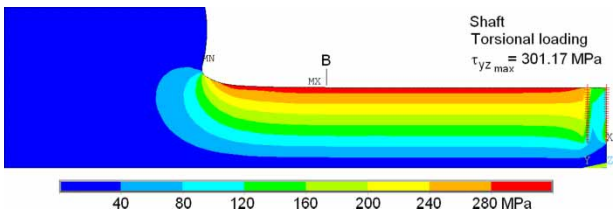

Fig. 20 Stress distribution developed in the optimal-shaped round bar with a 15-mm-shoulder fillet defined by three key points under torsion

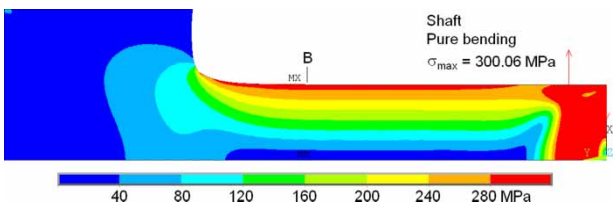

Fig. 21 Stress distribution developed in the optimal-shaped round bar with a 15-mm-shoulder fillet defined by three key points subject to pure bending moment

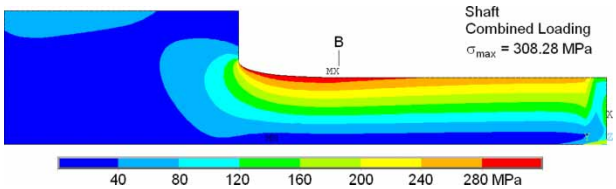

Fig. 22 Stress distribution developed in the optimal-shaped round bar with a 15-mm-shoulder fillet defined by five key points subject to both torsional and transverse loading

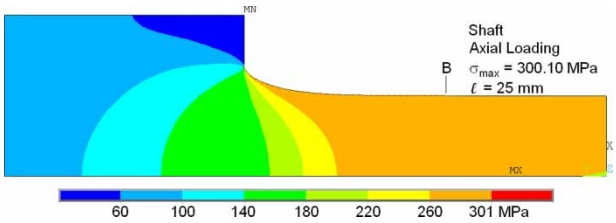

Fig. 23 Stress distribution developed in the axially loaded optimal-shaped round bar with a 25-mm-shoulder fillet defined by five key points

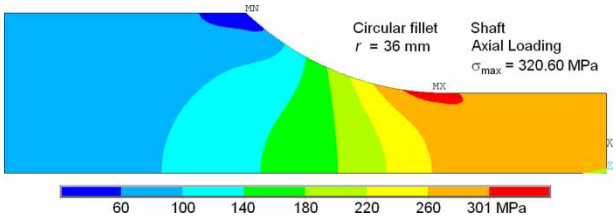

Fig. 24 Stress distribution developed in an axially loaded shouldered round bar with a circular fillet having 36-mm-radius of curvature

loaded region, pure bending moment develops inducing a stress state in which σ_{yy} component of stress has a maximum magnitude of 300.00 MPa. The corresponding equivalent stress is 299.25. The stress calculated by the formula $\sigma_{max} = Mc/I$ is 300.29 MPa. The slight difference is due to Poisson's effect neglected in the analytical formula. The maximum equivalent stress in the optimal-shaped beam is 300.06 MPa, which results in a stress concentration factor of 1.003. K_q of the circular fillet, on the other hand, is 1.103 with a maximum equivalent stress of 330.20 MPa.

Transmission shafts, which are susceptible to fatigue failure, are subjected to both torsional and transverse loading. Minimizing stress concentration at fillets is especially crucial in these applications. Accordingly, fillet shape of a shouldered shaft under combined loading was optimized. Figure 22 shows the resulting shape and the stress distribution. The shaft is subject to a torque (253.48 Nm) and a transverse force (2949.41 N) applied to the right end, which results in a nominal stress of magnitude equal to 300.00 MPa at point B, which is 4 cm away from the right end of the shaft. To avoid stress concentration at the point of application, the load was distributed to the nodes at the right end. The maximum equivalent stress in the optimal-shaped shaft is 308.28 MPa with $K_q = 1.028$. On the other hand, a circular fillet leads to a maximum stress of 333.24 MPa with $K_q = 1.110$.

One should note that optimal shapes for different types of loading are different. If the same pure torsional load is applied to the shaft optimized for combined loading, K_q increases about 1.0 per cent. The increase in K_q becomes 10 per cent, if the same combined load is applied to the shaft optimized for torsional loading.

To observe the dependence of the stress concentration factor on the transition length, the length of the search domain (the horizontal distance between A and B in Fig. 3) was increased to 25 mm, and the optimization process was repeated for an axially loaded round bar. Figure 23 shows the stress state. The maximum equivalent stress, which is 300.10 MPa, is virtually equal to the nominal stress, i.e. stress concentration is equal to one. This means that even for such a large reduction in the cross-section, the fillet having the optimal shape does not weaken the shaft. On the other hand, a circular fillet with 36 mm radius of curvature having about the same transition length (25 mm) results in a maximum stress of 320.60 MPa as shown in Fig. 24. Besides, comparison of Figs 18 and 23 indicates that an increase in the length of the transition region leads to a slight increase in the space occupied by the optimum fillet. The fillet area increases from

Table 2 Coordinates of the key points through which spline curve passes defining the optimal fillet boundary

Spline curve shown in	(x_1, y_1)	(x_2, y_2)	(x_3, y_3)	(x_4, y_4)	(x_5, y_5)	(x_6, y_6)	Angle
Figure 11	41.1409	38.2349	35.8601	32.0704	30.0010	35.4595	42.682
	10.2124	10.5943	11.0735	12.3073	14.3722	15.6969	
Figure 15	41.9795	39.0490	35.6326	32.7578	30.0003	37.3843	−42.673
	10.0002	10.0144	10.4729	11.2615	12.7898	14.8610	
Figure 17	53.8931	47.7525	41.3091	35.0092	30.2230	30.5169	136.752
	10.0903	10.3799	11.0679	12.4520	14.9337	16.4641	
Figure 18	10.1238	10.4869	11.5357	13.3359	14.4482		108.159
	34.9308	38.8308	42.9493	44.9998	43.8281		
Figure 20	10.1347	11.4635	14.1552				
	43.6399	49.9993	49.9997				
Figure 21	10.1512	11.4294	13.9530				
	48.1099	53.8341	54.9996				
Figure 22	10.1156	10.2836	11.0912	12.6993	15.8273		6.957
	44.7957	47.9762	53.0904	54.9987	53.5246		
Figure 23	10.0667	10.3598	12.2218	14.0687	13.4961		10.965
	30.4210	36.7073	43.9179	44.9987	44.0916		

9.5 to 11.6 mm^2. On the other hand, the circular fillet having 16 mm radius of curvature occupies an area of 41.0 mm^2 and 36 mm radius fillet occupies an area of 77.8 mm^2.

Table 2 gives the coordinates of the key points used to define spline curves describing the optimal fillet boundaries. Because spline curves can be constructed using maximum six key points in ANSYS, two spline curves were defined for the problems in which more than four moving key points were used. To ensure continuity of slope at the key point where the two spline curves are joined, the same angle was used for the line tangent to the curves at this key point. This angle is also an optimization variable and its optimum values are given in the table. The fifth moving key point was chosen as the connection point. It should also be noted that because y-axis should be chosen as the axisymmetry axis in ANSYS, the coordinate system is different from the one shown in Fig. 3 for the round bars.

5 CONCLUSIONS

In this study, global shape optimization of shoulder fillets in flat and round bars was achieved. Although optimum fillet design of flat bars was a problem that was considered by many researchers before, improved results were obtained in this study by applying a global shape optimization procedure. As for the optimum shape design of shouldered round bars, the results obtained in this study are remarkable. The stress concentration factors, K_q, in the optimal-shaped round bars were obtained to be 1.0 for axial, torsional, and pure bending load cases for the chosen geometry. For combined loading, K_q was close to 1.0. Therefore, use of this algorithm may significantly increase fatigue strength and reliability of machine parts.

Defining the boundary more precisely by using a larger number of key points yielded better optimal shapes. Increased precision posed difficulties for the algorithm to locate the globally optimal design accurately. To overcome this difficulty, a method was proposed to select a proper search domain. In this way, not only lower stress concentration factors were obtained in comparison to previous studies, but also accuracy and precision of the results were ensured.

Even though the transition length for the fillet is greatly increased, the region occupied by the optimal-shaped fillet increases slightly unlike circular fillets. For this reason, a large transition length can be chosen for the fillet without risking interference with another mechanical part as opposed to a circular fillet.

Optimal shapes were found to be different for different geometries as well as for different loading types (axial, torsional, bending, or any different combination of them). For this reason, the shape design optimization procedure should be reapplied for any new application.

If there is a geometric constraint such that the fillet boundary may not trespass into a predefined infeasible region at the shoulder, the stress along the boundary of the optimal-shaped fillet will not be constant. For this reason, commonly used methods to minimize stress concentration by trying to make the tangential stress uniform along the fillet boundary may not work if geometric constraints exist. Besides, tangential stress may also not be uniform in multi-objective shape optimization problems. The present method can easily be adapted to this type of problems.

The accuracy of finite-element calculations was shown to have a significant effect on the resulting optimized shape. If the error is not checked during shape optimization, the algorithm may lead to spurious optimal designs; as a result, the actual stress concentration in the optimized shape may be very high.

Using spline curves ensures smoothness of the boundary. As another advantage, manufacturing is easy because CNC machines use spline interpolation for free form surfaces.

ACKNOWLEDGEMENT

This article is based on the work supported by the Scientific Research Projects of Bogazici University with the code number 06A601.

REFERENCES

1 **Waldman, W., Heller, M.,** and **Chen, G. X.** Optimal free-form shapes for shoulder fillets in flat plates under tension and bending. *Int. J. Fatigue*, 2001, **23**, 509–523.
2 **Francavilla, A., Ramakrishnan, C. V.,** and **Zienkiewicz, O. C.** Optimization of shape to minimize stress concentration. *J. Strain Analysis*, 1975, **10**(2), 63–70. DOI: 10.1243/0309324V102063.
3 **Kristensen, E. S.** and **Madsen, N. F.** On the optimum shape of fillets in plates cases subjected to multiple in-plane loading cases. *Int. J. Numer. Methods Eng.*, 1976, **10**, 1007–1019.
4 **Bhavikatti, S. S.** and **Ramakrishnan, C. V.** Optimum shape design of shoulder fillets in tension bars and T-heads. *Int. J. Mech. Sci.*, 1979, **21**(1), 29–39.
5 **Queau, J. P.** and **Trompette, P. H.** Two-dimensional shape optimal design by the finite element method. *Int. J. Numer. Methods Eng.*, 1980, **15**, 1603–1612.
6 **Pedersen, P.** and **Laursen, C. L.** Design for minimum stress concentration by finite element and linear programming. *J. Struct. Mech.*, 1982–83, **10**(4), 375–391.
7 **Schnack, E.** and **Sporl, U.** A mechanical dynamic programming algorithm for structure optimization. *Int. J. Numer. Methods Eng.*, 1986, **23**, 1985–2004.
8 **Andrews, J. D.** and **Hearn, J.** An automatic design optimization procedure to minimize fillet bending stresses in involute spur gears. *Int. J. Numer. Methods Eng.*, 1987, **24**, 975–991.

9 **Shyy, Y. K., Fleury, C.,** and **Izadpanah, K.** Shape optimal design using high-order elements. *Comput. Methods Appl. Mech. Eng.*, 1988, **71**, 99–116.

10 **Choi, J. H.** and **Kwak, B. M.** Boundary integral equation method for shape optimization of elastic structures. *Int. J. Numer. Methods Eng.*, 1988, **26**, 1579–1595.

11 **Yang, R. J.** Component shape optimization using BEM. *Comput. Struct.*, 1990, **37**(4), 561–568.

12 **Andrews, J. D.** A Design optimization procedure to minimize fillet bending stresses in an epicyclic gear system. *Int. J. Numer. Methods Eng.*, 1991, **31**, 859–878.

13 **Shim, P. Y.** and **Manoochehri, S.** Generating optimal configurations in structural design using simulated annealing. *Int. J. Numer. Methods Eng.*, 1997, **40**, 1053–1069.

14 **Wilczynski, B.** Shape optimisation for stress reduction around single and interacting notches based on the fictitious stress method. *Eng. Anal. Bound. Elem.*, 1997, **19**, 117–128.

15 **Phan, A.-V., Mukherjee, S.,** and **Mayer, J. R. R.** Stresses, stress sensitivities and shape optimization in two-dimensional linear elasticity by the boundary contour method. *Int. J. Numer. Methods Eng.*, 1998, **42**, 1391–1407.

16 **Wang, X., Zhou, J.,** and **Hu, Y.** A physics-based parameterization method for shape optimization. *Comput. Methods Appl. Mech. Eng.*, 1999, **175**, 41–51.

17 **Phan, A.-V.** and **Phan, T.-N.** A Structural shape optimization system using the two-dimensional boundary contour method. *Arch. Appl. Mech.*, 1999, **69**, 481–489.

18 **Li, Q., Steven, G. P., Querin, O. M.,** and **Xie, Y. M.** Evolutionary shape optimization for stress minimization. *Mech. Res. Commun.*, 1999, **26**(6), 657–664.

19 **Pedersen, P.** On optimal shapes in materials and structures. *Struct. Multidiscip. Optim.*, 2000, **19**, 169–182.

20 **Hedia, H. S.** Shape optimisation to maximize crack initiation time. *Bio-Med. Mater. Eng.*, 2001, **11**, 293–300.

21 **Bobaru, F.** and **Mukherjee, S.** Shape sensitivity analysis and shape optimization in planar elasticity using the element-free Galerkin method. *Comput. Methods Appl. Mech. Eng.*, 2001, **190**, 4319–4337.

22 **Freitas, J. A. T.** and **Cismasiu, I.** Shape optimization with hybrid – Trefftz displacement elements. *Int. J. Numer. Methods Eng.*, 2002, **53**, 473–498.

23 **Parvizian, J.** and **Fenner, R. T.** Shape optimization of fillets by the boundary element method. *J. Strain Analysis*, 2002, **37**(2), 93–100. DOI: 10.1243/0309324021514862.

24 **Jones, R., Chaperon, P.,** and **Heller, M.** Structural optimisation with fracture strength constraints. *Eng. Fract. Mech.*, 2002, **69**, 1403–1423.

25 **Jang, G.-W., Kim, Y. Y.,** and **Choi, K. K.** Remesh-free shape optimization using the Wavelet–Galerkin method. *Int. J. Solids Struct.*, 2004, **41**, 6465–6483.

26 **Wessel, C., Cisilino, A.,** and **Sensale, B.** Structural shape optimisation using boundary elements and the biological growth method. *Struct. Multidiscip. Optim.*, 2004, **28**, 221–227.

27 **Das, R., Jones, R.,** and **Xie, Y. M.** Design of structures for optimal static strength using ESO. *Eng. Fail. Anal.*, 2005, **12**, 61–80.

28 **Jones, R., Peng, D., Chaperon, P., Pitt, S., Abramson, D.,** and **Peachey, T.** Structural optimisation with damage tolerance constraints. *Theor. Appl. Fract. Mech.*, 2005, **43**, 133–155.

29 **Wu, Z.** An efficient approach for shape optimization of components. *Int. J. Mech. Sci.*, 2005, **47**, 1595–1610.

30 **Mattheck, C.** Teacher tree: the evolution of notch shape optimization from complex to simple. *Eng. Fract. Mech.*, 2006, **73**, 1732–1742.

31 **Klemenso, T., Lund, E.,** and **Sorensen, B. F.** Optimal shape of thin tensile test specimen. *J. Am. Ceram. Soc.*, 2007, **90**(6), 1827–1835.

32 **Spitas, V.** and **Spitas, C.** Optimizing involute gear design for maximum bending strength and equivalent pitting resistance. *Proc. IMechE, Part C: J. Mechanical Engineering Science*, 2007, **221**(C4), 479–488. DOI: 10.1243/0954406JMES342.

33 **Miegroet, L. V.** and **Duysinx, P.** Stress concentration minimization of 2D fillets using X-FEM and level set description. *Struct. Multidiscip. Optim.*, 2007, **33**, 425–438.

34 **Zhang, X., Rayasam, M.,** and **Subbarayan, G.** A meshless, compositional approach to shape optimal design. *Comput. Methods Appl. Mech. Eng.*, 2007, **196**, 2130–2146.

35 **Pedersen, P.** Suggested benchmarks for shape optimization for minimum stress concentration. *Struct. Multidiscip. Optim.*, 2008, **35**, 273–283.

36 **Noda, N.-A., Takase, Y.,** and **Monda, K.** Stress concentration factors for shoulder fillets in round and flat bars under various loads. *Int. J. Fatigue*, 1997, **19**(1), 75–84.

37 **Sonmez, F. O.** Shape optimization of 2D structures using simulated annealing. *Comput. Methods Appl. Mech. Eng.*, 2007, **196**(35–36), 3279–3299.

38 **Sonmez, F. O.** Structural optimization using simulated annealing. In *Simulated annealing* (Ed. C. M. Tan), 2008, pp. 281–306 (I-Tech Education and Publishing, Vienna).

39 **Ali, M. M., Törn, A.,** and **Viitanen, S.** A direct search variant of the simulated annealing algorithm for optimization involving continuous variables. *Comput. Oper. Res.*, 2002, **29**, 87–102.

40 **Tipton, S. M., Sorem, Jr, J. R.,** and **Rolovic, R. D.** Updated stress concentration factors for filleted shafts in tension and bending. *ASME J. Mech. Des.*, 1996, **118**, 321–327.

41 **Rolovic, R. D., Tipton, S. M.,** and **Sorem, Jr, J. R.** Multiaxial stress concentration in filleted shafts. *ASME J. Mech. Des.*, 2001, **123**, 300–303.

APPENDIX

Notation

d	smaller diameter of round bar or smaller width of flat bar
D	larger diameter of round bar or larger width of flat bar
f	objective function to be minimized
f_{h}	highest objective function value of the current configurations
f_{l}	lowest objective function value of the current configurations
f_{t}	objective function value of the newly generated configuration
K_{q}	stress concentration factor defined based on the equivalent stress
K_{t}	stress concentration factor defined based on the first principal stress

L	Markow chain length (i.e. number of iterations in an inner loop)	S_{nom}	normal component of nominal stress
n	number of optimization variables	T	temperature parameter of the simulated annealing process
N	number of initial configurations	σ_{q}	equivalent stress
$R_{\max}$	maximum moving distance of key points	τ_{nom}	shear component of nominal stress